hydrology

MDPI

Article

Comparative Assessment of Different Satellite-Derived Actual Evapotranspiration Estimates in Northeast Italy

Marta Chiesi [1], Sofia Ortenzi [2], Paulina Bartkowiak [3], Matteo Camporese [4], Mariapina Castelli [3], Jacopo Dari [2,5], Luca Fibbi [1,6], Beatrice Gatto [4], Christian Massari [2], Maurizio Pieri [1], Silvana Vanucci [7] and Fabio Maselli [1,*]

1 Institute of BioEconomy, National Research Council (CNR-IBE), 50019 Sesto Fiorentino, Italy; marta.chiesi@cnr.it (M.C.); luca.fibbi@cnr.it (L.F.); maurizio.pieri@cnr.it (M.P.)
2 Research Institute for Geo-Hydrological Protection, National Research Council (CNR-IRPI), 06128 Perugia, Italy; sofia.ortenzi@cnr.it (S.O.); jacopo.dari@unipg.it (J.D.); christian.massari@cnr.it (C.M.)
3 Eurac Research Institute for Earth Observation, 39100 Bolzano, Italy; paulina.bartkowiak@eurac.edu (P.B.); mariapina.castelli@eurac.edu (M.C.)
4 Department of Civil, Environmental and Architectural Engineering, University of Padua (UNIPD), 35131 Padova, Italy; matteo.camporese@unipd.it (M.C.); beatrice.gatto@unipd.it (B.G.)
5 Department of Civil and Environmental Engineering, University of Perugia (UNIPG), 06125 Perugia, Italy
6 LaMMA Consortium, 50019 Sesto Fiorentino, Italy
7 Department of Chemical, Biological, Pharmaceutical and Environmental Sciences, University of Messina (UNIME), 98166 Messina, Italy; silvana.vanucci@unime.it
* Correspondence: fabio.maselli@cnr.it

Abstract

Accurate estimation of actual evapotranspiration (ETa) is essential for understanding hydrological processes and managing water resources, especially in regions characterized by intensive agriculture and complex groundwater–surface interactions. This study intercompares three independent satellite-based ETa estimation approaches applied over Northeast Italy. The first two methods correspond to the classical MODIS algorithm (MOD16), which is based on a simplified Penman–Monteith approach, and to the more recent Sen-ET modelling framework, which relies on a surface energy balance principle. The outputs of these methods are compared to those produced by a water balance algorithm, NDVI-Cws, which predicts ETa through the combination of conventional ancillary data and MODIS NDVI imagery. The results obtained show that, while the MODIS algorithm yields ETa estimates which are generally lower than those of Sen-ET and NDVI-Cws, the latter methods produce similar predictions for most cover types examined. The same two methods are potentially capable of providing higher spatial resolution daily ETa estimates depending on the satellite inputs used; out of them, however, only NDVI-Cws can yield spatially complete and temporally continuous datasets. The analysis therefore provides insights into the reliability and usability of different remote sensing approaches for regional-scale water resource monitoring.

Keywords: MOD16; Sen-ET; NDVI-Cws; water stress; croplands; forests

Check for updates

Academic Editors: Pooja P. Preetha, Changsen Zhao and Leszek Sobkowiak

Received: 31 March 2026
Revised: 7 May 2026
Accepted: 26 May 2026
Published: 29 May 2026

Copyright: © 2026 by the authors. Licensee MDPI, Basel, Switzerland. This article is an open access article distributed under the terms and conditions of the Creative Commons Attribution (CC BY) license.

1. Introduction

Actual evapotranspiration (ETa) represents the combined flux of water vapour from soil evaporation and plant transpiration under real environmental and physiological conditions. ETa constitutes a major component of the terrestrial water cycle and plays a key role in soil moisture dynamics, which in turn controls the partitioning of precipitation into

runoff, infiltration, and atmospheric return. Because it integrates the effects of climate, soil properties, vegetation characteristics and land management, ETa plays a central role in hydrological processes and ecosystem functioning [1]. Accurate quantification of ETa is therefore essential for sustainable water resources management, particularly in agricultural regions where water availability can be a major limiting factor for crop productivity [2]. ETa monitoring at appropriate spatial and temporal scales, in fact, enables the assessment of water balance dynamics at catchment and regional levels as well as informed decision-making regarding the allocation of water to different sectors.

The operational estimation of ETa over large areas is, however, a complex task, since this process is highly variable in both space and time, particularly in fragmented and heterogenous landscapes. Remote sensing techniques are intrinsically suitable for estimating land surface properties that can be useful for ETa prediction, and this property has been enhanced in recent years by the availability of datasets acquired by new satellite systems. Numerous remote sensing algorithms have therefore been proposed for ETa prediction at different spatial and temporal scales, which are generally categorized into surface energy balance, surface water balance and mixed methods [3,4].

Energy balance methods rely on the estimation of land surface temperature (LST) and can directly assess ETa; these methods, however, are difficult to apply for the operational monitoring of large, heterogeneous areas due to the coarse spatial resolution and the low temporal frequency of undisturbed thermal infrared (TIR) imagery [5]. These issues have been partly addressed by the use of data fusion procedures that merge TIR and optical imagery. This is the case of the OpenET products, which offer high spatial resolution (up to 30 m) but a reduced temporal frequency (usually around one month) [6]. Similarly, the standard algorithm applied by the Copernicus Project based on Sentinel-2 (S-2) and Sentinel-3 (S-3) constellations, i.e., Sentinels for Evapotranspiration (Sen-ET), produces discontinuous ETa estimates at 20 m spatial resolution [7].

The necessity for operational, spatially and temporally complete ETa datasets is therefore still usually addressed through mixed methods. The most well-known example of these is represented by the MODIS algorithm (MOD16), which yields global ETa estimates through a simplified Penman–Monteith approach [8]. The MOD16 product, however, has relevant spatio-temporal limitations, being produced at 500 m resolution over 8-day periods, and presents sub-optimal performances in arid and semi-arid regions [9].

An alternative is offered by water balance methods, which rely on the resource optimization theory to track the pathways of rainfall within the soil–vegetation system [3,5]. These methods predict ETa by combining indicators of green foliage biomass, such as the well-known Normalized Difference Vegetation Index (NDVI), with estimates of potential evapotranspiration (ET_0). In practice, NDVI or other vegetation indices replace the use of time-varying crop coefficients (Kc), which, requiring the knowledge of the crop planted in each field and its calendar, is impractical for the monitoring of large areas [10,11].

Optical observations, however, are only partly sensitive to water stress (WS), which initially induces transient and reversible plant adaptation mechanisms and only subsequently leads to substantial green biomass decreases [12]. As a consequence, classical water balance methods must rely on the basic assumption that the observed vegetation is growing under unstressed water conditions [5]. These methods are therefore efficient in regions where WS is scarce (i.e., in humid or irrigated areas) but can produce substantial overestimation in arid or semi-arid environments [5].

The extension of these methods to water-limited ecosystems is generally performed by the use of additional environmental information. The Veg-ET model developed by Senay et al. [13], for example, includes a scalar similar to the FAO Ks coefficient derived from a site water balance that requires information on soil properties. The common scarcity

of such information is circumvented in the NDVI-Cws method [14] by the proper elaboration of meteorological inputs. This method, in fact, operates through the combination of conventional weather data and satellite NDVI images, which are used to simulate the effect of transient and persistent WS, respectively [14]. The NDVI-Cws method has been tested in several investigations, which have also addressed some shortcomings that can limit its usage in specific cases. The proposed advancements have rendered the method potentially applicable for operational ETa monitoring with a spatial resolution that is mainly constrained by the NDVI imagery used.

In summary, all three mentioned remote sensing ETa estimation strategies present pros and cons that should be carefully evaluated case by case. This operation is, however, constrained by the common scarcity of ground references having the appropriate spatial and temporal resolutions, i.e., a pixel size of tens of metre and daily temporal frequency. For example, the eddy covariance technique, which is the most common method to produce continuous ETa measurements, is applicable only on regular terrains and provides observations referred to relatively large (and uncertain) footprint areas [15].

An alternative to the use of ground observations is offered by the intercomparison of different estimated datasets, which can provide insights into the consistency and relative reliability of each prediction method [16]. This strategy allows the identification of systematic differences and common patterns among the datasets and is particularly useful when independent measurements are not available. This is the case for a relatively large region in Northeast Italy, covered by semi-natural and agricultural surfaces, the latter grown both in rainfed and irrigated conditions. The area is characterized by an extremely fragmented and heterogeneous mosaic of the cover types, which enhances its representativity for other environmentally complex European regions.

The datasets currently analyzed are representative of the three basic ETa estimation strategies previously described. The first corresponds to the standard MODIS ETa product, while the others are obtained through advanced energy and water balance methods, i.e., the Sen-ET and NDVI-Cws algorithms, respectively. The specific objective of this study is to evaluate the consistency and uncertainty of ETa estimates obtained from the three methods to support sustainable water resource management in the study area. The identification of the strengths and limitations of each approach, in fact, can provide guidance for local water resource managers and agricultural practitioners regarding the most appropriate methods for operational application.

The remainder of this paper is organized as follows. Section 2 describes the study area and data, followed by the algorithms used for producing the three ETa datasets and the processing steps applied for their intercomparison. Section 3 presents the results obtained during these operations, which are discussed in Section 4. Finally, Section 5 provides conclusions and identifies future research prospects for improving ETa estimation in fragmented and heterogeneous regions.

2. Materials and Methods

2.1. Study Area

The study area is located in the Veneto Region (Northeast Italy), and more precisely in the high and middle sectors of the Venetian plain (Figure 1). This area covers approximately 900 km^2 and has an altitude ranging from about 50 m a.s.l. in the South to 400 m a.s.l. in the North [17]. The climate is continental humid, with mean annual temperature around 13 °C and annual precipitation around 1000 mm. The land is mostly covered by mixed forests in the North and by annual and perennial crops in the rest of the area; most summer crops, such as corn and vegetables, are regularly irrigated, while emergency irrigation is usually applied to vineyards. All these characteristics make the area particularly suitable

for investigating ETa variability as observed by remote sensing datasets. This operation, however, cannot rely on ground ETa measurements, which are not currently available for this portion of the Venetian plain.

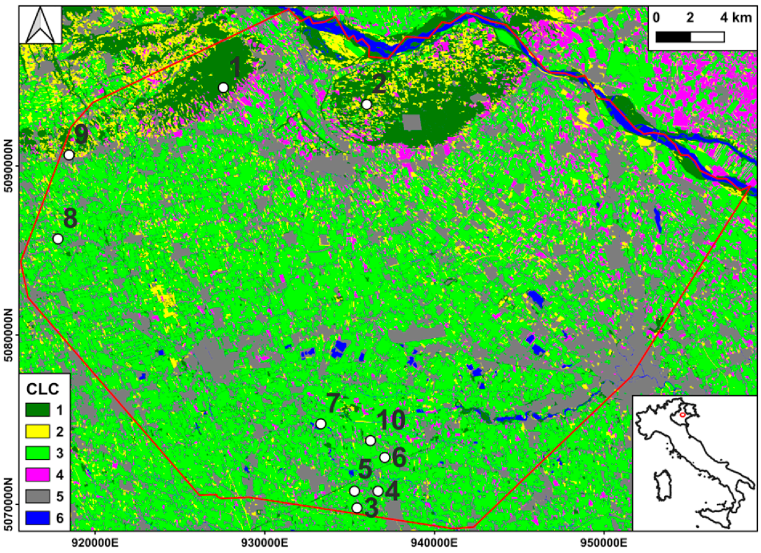


Figure 1. Land cover map of the study area (1 = forests, 2 = grasslands, 3 = annual crops, 4 = perennial crops, 5 = urban lands, 6 = water bodies); the red line indicates the boundary of the area examined and the white circles the location of the ten test sites. The lower-right box indicates the geographical position of the study area in Italy.

2.2. Model Drivers

2.2.1. Sen-ET

The input variables of Sen-ET can be aggregated into three main categories: optical and biophysical variables from S-2 Multi Spectral Imager, thermal images from S-3 Sea and Land Surface Temperature Radiometer (SLSTR), and meteorological forcings from European Reanalysis V5 (ERA5).

S-2 Level-2A surface reflectance in the visible to short-wave infrared spectrum, resampled to 100 m, drives the retrieval of key canopy biophysical variables, including leaf area index (LAI), fraction of Absorbed Photosynthetically Active Radiation (fAPAR), and fractional green vegetation cover (f_G). Land surface temperature (LST), as a main driver of the Priestley–Taylor two-source energy balance (TSEB-PT) model, was obtained from the S-3 SLSTR Level 2 product at 1 km resolution, with acquisitions at the lowest viewing zenith angle to reduce angular anisotropy effects [18].

Apart from satellite-based forcings, surface energy balance closure relies on ERA5 reanalysis fields, including air temperature, vapour pressure, wind speed, surface pressure, and solar radiation components, all matched to S-3 acquisition times [19]. ERA5 variables were corrected for terrain effects using a digital elevation model (DEM) and adjusted to a 100 m blending height [7]. In this regard, the 90 m Shuttle Radar Topography Mission (SRTM) DEM was utilized for topographic correction for ERA5 and as a predictor in the LST sharpening procedure, while 300 m Copernicus Climate Change Initiative land cover maps provided vegetation structural parameters for TSEB-PT, as explained in Section 2.4 [20,21].

2.2.2. NDVI-Cws

Daily precipitation and air temperature data were obtained from the *Agenzia Regionale per la Prevenzione e Protezione Ambientale del Veneto* and are based on observations from 20 meteorological stations distributed within and around the study area. The precipitation data were spatially interpolated on the reference grid using the inverse distance

weighting method, following the formulation recommended by the World Meteorological Organization [22].

Solar radiation was instead obtained by means of the ERAD algorithm which is based on the use of the Meteosat Second Generation imagery [23]. All daily meteorological data are available at 250 m spatial resolution over the years 2019–2021.

A land cover map of the same area was obtained from the CORINE Land Cover (CLC) database. The original CLC classes were regrouped to identify the following categories: forests, grasslands, annual crops, perennial crops, urban lands and water bodies (Figure 1). Half of this area (50%) is covered by annual crops followed by urban lands (27%) while forests, grasslands, perennial crops and water bodies represent the 9%, 7%, 6%, and 1% of it, respectively.

MODIS NDVI images collected by the Terra and Aqua sensors were obtained from the NASA Land Processes Distributed Active Archive Center (LP DAAC). The present work uses the MOD13Q1 product, which is provided as a maximum value composite (MVC) every 16 days, at a 250 m spatial resolution. All images of the tile corresponding to the Venetian plain (i.e., 23 NDVI MVC images per year) were downloaded from the NASA website (https://lpdaac.usgs.gov/; accessed on 16 March 2026) for the whole study period (2019–2021).

2.3. ETa Estimation Methods

2.3.1. MOD16

The MOD16A2GF product is an improved, gap-filled version of the global MODIS terrestrial evapotranspiration dataset [24]. It provides ETa estimates at a spatial resolution of approximately 500 m and a temporal resolution of 8 days, covering vegetated land areas globally since the year 2000. The dataset is based on the MOD16 algorithm, which relies on the Penman–Monteith equation. This approach integrates daily meteorological reanalysis data with vegetation biophysical parameters derived from MODIS optical observations, such as LAI, fAPAR and surface albedo [8,25].

ETa is partitioned into its main physical components: soil evaporation, evaporation from wet canopy surfaces and plant transpiration. The model operates at a daily time step, and the fluxes are then aggregated into 8-day composites. A key limitation of the standard MOD16 products is the contamination of input data by clouds and aerosols. This issue can lead to missing or unreliable values, especially in regions with persistent cloud cover. To reduce this limitation, the MOD16A2GF product introduces an annual gap-filling procedure that corrects, or replaces, low-quality or missing input data relying on temporal interpolation and multi-year climatologies. The MOD16A2GF product is not available in near real-time, as it is generated only after the end of each year, when all necessary observations are collected and processed; it is distributed into tiles, each of them representing an area of approximately $10^\circ \times 10^\circ$ latitude/longitude.

2.3.2. Sen-ET

The Sen-ET project aimed at developing an optimal methodology for estimating sub-kilometre ETa, based on synergistic use of S-2 and S-3 observations through energy balance modelling. Within this framework, the TSEB-PT estimates ETa by partitioning the surface energy balance between soil (S) and canopy (C) layers separately [26,27]. Unlike single-source approaches, TSEB-PT treats the land surface as two distinct layers, solving the energy balance for each component independently, as shown in the equations below:

$$Rn_S = H_S + LE_S + G \quad (1)$$

$$Rn_C = H_C + LE_C \quad (2)$$

where Rn is net radiation (W m^{-2}), LE is latent heat flux (W m^{-2}), H is sensible heat flux (W m^{-2}), and G is soil heat flux (W m^{-2}).

The partitioning of energy between S and C components relies on two primary remote sensing inputs: LST, which represents the combined radiometric temperature of the surface, and f_G derived from LAI. Canopy transpiration (LE_C) is first estimated using the Priestley–Taylor approximation [28] (Priestley and Taylor, 1972):

$$LE_C = \left[\alpha_{PT} \cdot f_G \cdot \frac{\Delta}{\Delta + \gamma}\right] \cdot Rn_C \quad (3)$$

where α_{PT} is the Priestley–Taylor coefficient (default value 1.26), f_G is the fraction of green vegetation, Δ (kPa K^{-1}) and γ (kPa K^{-1}) are the slope of the vapour pressure curve and the psychrometric constant, respectively. Next, LE_S is calculated as a residual of the overall energy balance ($LE_S = Rn_S - H_S - G$). TSEB-PT then iteratively decomposes LST into soil and canopy temperatures using fractional vegetation cover as a weighting factor, with sensible and soil heat fluxes derived as residual terms of the energy balance [26]. Instantaneous latent heat flux estimates at S-3 overpass times are extrapolated to daily ET using all-sky ERA5 daily solar radiation.

Further details on the TSEB-PT formulation and its implementation can be found in Guzinski et al. [7], Chintala et al. [29] and Bartkowiak et al. [30] as well as in the open-source pyTSEB Python library (https://github.com/hectornieto/pyTSEB; accessed on 19 March 2026). An abbreviation list explaining all algorithm variables is provided at the end of the manuscript followed by a scheme of the algorithm functioning (Figure A1).

2.3.3. NDVI-Cws

The NDVI-Cws method developed by Maselli et al. [14,31] uses the fractional vegetation cover (FVC) concept to separate the contribution of evaporating and transpiring surfaces, and it is therefore capable of estimating the ETa of day *i*, ETa_i, through the following formula:

$$ETa_i = ET_{0i} \cdot (Kc_{Veg} \cdot FVC_i \cdot (0.5 + 0.5 \cdot AW_i) + Kc_{Soil} \cdot (1 - FVC_i) \cdot AW_i) \quad (4)$$

where ET_0 is potential evapotranspiration obtained from air temperature and solar radiation using the Jensen and Heise [32] algorithm, Kc_{Veg} and Kc_{Soil} are the maximum crop coefficients for vegetation and soil, respectively [1], FVC is linearly derived from NDVI according to Gutman and Ignatov [33], and AW is a daily meteorological WS scalar computed as:

$$AW_i = Rain/ET_0 \quad (5)$$

where rainfall and ET_0 are cumulated over periods diversified for plant functional types and the ratio is bounded to 1, so that AW can vary between 0 (full WS) and 1 (no WS). According to the theoretical background of this method, the AW scalar takes into account the effect of short-term WS, which induces only marginal green biomass decrease, while FVC accounts for the long-term impact of WS [12,14].

The WS scalar must therefore be deactivated for irrigated crops, i.e., when water additional to rainfall is supplied. To fulfil this objective, Maselli et al. [31] introduced a methodological modification that is applicable to potentially irrigated crops during the summer dry period. The modification relies on the joint evaluation of AW and FVC variations and induces a deactivation of the meteorological WS scalar when a disequilibrium is detected between natural water supply and plant development. This temporary deactivation allows for the prediction of ETa in the fully watered condition that is presumed to occur when irrigation is applied.

2.4. Data Processing

The MOD16A2GF ETa tile covering the whole Venetian plain was downloaded from the NASA website for the years 2019–2021. All these images were then reprojected to the reference system of the MODIS NDVI imagery (i.e., 250 m) by a nearest neighbour algorithm.

The Sen-ET evapotranspiration processing pipeline was implemented in order to produce daily 100 m ETa maps over the study area for the period 2019–2021 by combining S-2 biophysical variables, downscaled 100 m S-3 LST, and ERA5 meteorological forcing. Biophysical variables, including LAI and fAPAR, were retrieved from S-2 at 100 m spatial resolution using the S-2 Toolbox Biophysical Processor [34]. Biophysical outputs were composited over 10-day temporal windows to ensure temporal consistency with daytime S-3 acquisitions and minimize cloud contamination [30,35]. To resolve surface heterogeneity within 1 km pixels, S-3 LST was downscaled to 100 m using the data mining sharpener algorithm with embedded decision trees [36,37], which combines global and local regression models relating coarse LST to S-2 reflectances and SRTM-derived topographic variables, with energy conservation enforced through residual correction [38]. TSEB-PT was run for each S-3 acquisition to derive instantaneous energy fluxes at 100 m resolution, which were subsequently extrapolated to daily ETa. Daily ETa maps were then generated as mosaics by averaging overlapping S-2 tile-based ETa grids (https://sentiwiki.copernicus.eu/web/s2-products; accessed on 19 March 2026), with invalid pixels due to cloud cover, non-land surfaces, and missing input data masked out. All mosaics were re-projected onto the same coordinate system used for the MODIS NDVI imagery, i.e., at 250 m spatial resolution [39].

The version of the NDVI-Cws algorithm that takes into account the possible water supplied to annual and perennial crops by irrigation was also applied for the same area and years. The method was driven by the available ancillary datasets and MODIS MVC NDVI imagery as fully described in Chiesi et al. [40]. Daily estimates of ETa at 250 m spatial resolution were thus obtained over the entire study region and period.

2.5. Evaluation of the Three Datasets

The evaluation of the MOD16, Sen-ET and NDVI-Cws ETa outputs was performed taking into consideration their different spatio-temporal characteristics. In fact, only the estimates produced by NDVI-Cws were available on a daily basis for the whole study area and period. The MODIS ETa product was instead aggregated over 8 days, while the estimates yielded by Sen-ET were discontinuous, i.e., irregularly covered the study area in different days. The assessment of the three datasets was therefore carried out over ten sites corresponding to pixels which had the maximum density of Sen-ET estimates and were representative of different vegetation types; the geographical position of these pixels is shown in Figure 1, and their main environmental features are summarized in Table 1. While the selected sites do not fully capture the spatial variability of the entire study area, they provide a representative sample of the main land cover types and ensure sufficiently complete and consistent time series for a robust intercomparison among datasets.

The ETa estimates of each site were extracted from the three datasets and were subjected to dual intercomparisons, i.e., the NDVI-Cws estimates were separately compared to their MOD16 and Sen-ET counterparts. In the former case all values aggregated over 8-day periods were considered, while in the latter case only days with Sen-ET values were taken into consideration; no comparison was carried out directly between MOD16 and Sen-ET estimates because of their spatio-temporal mismatching.

A first analysis concerned the ETa averages obtained in this way for the ten selected sites. Next, the accordance between the estimates was quantified through the reduced major axis (RMA) regression technique. As reported by Harper [41], the use of RMA regression is preferable to its ordinary least square counterpart when the X and Y variables

are fundamentally equivalent and similarly affected by errors. RMA regressions were therefore applied for separately intercomparing the MOD16 and NDVI-Cws and the Sen-ET and NDVI-Cws estimates of each site, summarizing the results through the coefficient of determination (r^2) and the regression slope (a) and intercept (b).

3. Results

Out of the selected test sites, two are mainly covered by forests, six by annual crops and two by mixtures of annual crops with perennial crops and grasses (Table 1). The mean annual rainfalls of these sites vary from 980 to 1200 mm and are slightly lower than the respective annual ET_0 in seven out of ten sites. This confirms the continental humid nature of the study area, where only a marginal water deficit usually occurs during the hottest summer months.

While both the MOD16 and NDVI-Cws methods provide temporally continuous ETa estimates for the whole study period, this is not the case for the Sen-ET algorithm. The numbers of available daily Sen-ET estimates obtained over the ten test sites, in fact, range from 452 to 463 over three years, which corresponds to about 43% of the total. These numbers are of course higher than the average calculated over the whole study area, which is around 30%. The days with missing values are irregularly distributed during the year and are often consecutive, particularly during fall and winter periods.

The ETa averages obtained applying the three methods over the ten selected sites are shown in Figure 2a,b. The values in Figure 2b are generally higher than those of Figure 2a due to the previously mentioned preferential occurrence of Sen-ET estimates in sunny days and during the growing season, when ETa is generally highest.

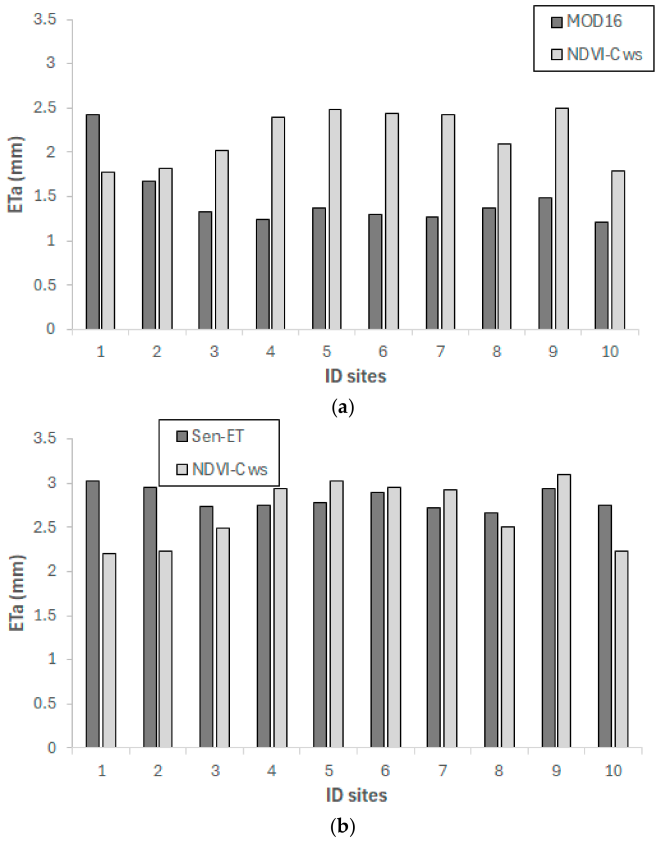


Figure 2. Histograms of daily ETa averages estimated by MOD16 and NDVI-Cws (**a**) and by Sen-ET and NDVI-Cws (**b**) for the ten test sites. In Figure 2b the averages are calculated considering only the days with Sen-ET estimates.

All ETa averages of MOD16 are notably lower than the respective NDVI-Cws averages, with the exception of the first forest site (site 1). This implies that the difference between these averages is statistically significant from Student's *t*-test ($p < 0.05$); a highly significant difference ($p < 0.01$) is obtained by applying the same test to the eight non-forest sites (i.e., for areas covered by annual and perennial, partially irrigated crops).

The mean ETa estimates of the same sites predicted by Sen-ET and NDVI-Cws are instead similar: the Sen-ET averages are higher than the corresponding NDVI-Cws values for the two forest sites and in other three cases, while the opposite is true for the remaining cases. The differences between these averages are not significant from Student's *t*-test, both considering all ten sites and only the eight non-forest sites.

Table 1. Geographical position, main meteorolsogical features including ET_0 computed using air temperature and solar radiation following Jensen and Haise [32], and prevalent CORINE Land Cover (CLC) class of the ten sites selected for the ETa intercomparisons. The underscored IDs correspond to the sites for which statistics are shown in Figures 3 and 4, while those for the others are reported in Table 2.

ID	° Lat. N	° Long. E	ET_0 (mm)	Precipitation (mm)	Prevalent CLC Class
1	45.8170	11.9688	1010	1152	Forest
2	45.8080	12.0759	1125	1111	Forest
3	45.5938	12.0223	1145	1002	Grassland
4	45.6027	12.0402	1143	1013	Annual crop
5	45.6027	12.0223	1138	976	Annual crop
6	45.6205	12.0491	1147	1041	Annual crop
7	45.6384	12.0045	1135	1066	Annual crop
8	45.7366	11.8259	1116	1158	Annual crop
9	45.7813	11.8438	1095	1199	Perennial crop
10	45.6295	12.0402	1134	1074	Perennial crop

These patterns can be better interpreted by looking at the scatter plots of four representative sites (Figures 3 and 4), the first covered by forest and the others by annual crops mixed with grasses and perennial crops in the first and third cases, respectively. Figure 3a–d exemplifies the accordance between MOD16 and NDVI-Cws estimates aggregated over 8-day periods; the correlations are high in all cases, but the regression statistics confirm the great ETa differences noted in Figure 2a, with the same exception of the forest site. The scatter plots of Figure 4 instead indicate a substantial agreement between the available daily Sen-ET and NDVI-Cws estimates for all cover types, both in terms of correlation and regression statistics.

These results are confirmed by the regression statistics of the other six sites reported in Table 2. With the exception of forest, all reduced major axis slopes between MOD16 and NDVI-Cws estimates are higher than 2.9 (Table 2a). The case is different for the intercomparisons between Sen-ET and NDVI-Cws estimates, which yield much lower regression slopes ranging from 0.96 to 1.68 (Table 2b).

In general, the different spatial and temporal properties of the intercomparisons made are expected to affect only marginally the statistics describing the quantitative concordance among ETa datasets, i.e., the averages and the regression intercepts and slopes obtained. These statistics indicate that the NDVI-Cws estimates are quantitatively less similar to the MOD16 than to the Sen-ET estimates, which would also imply a low similarity between the latter two products.

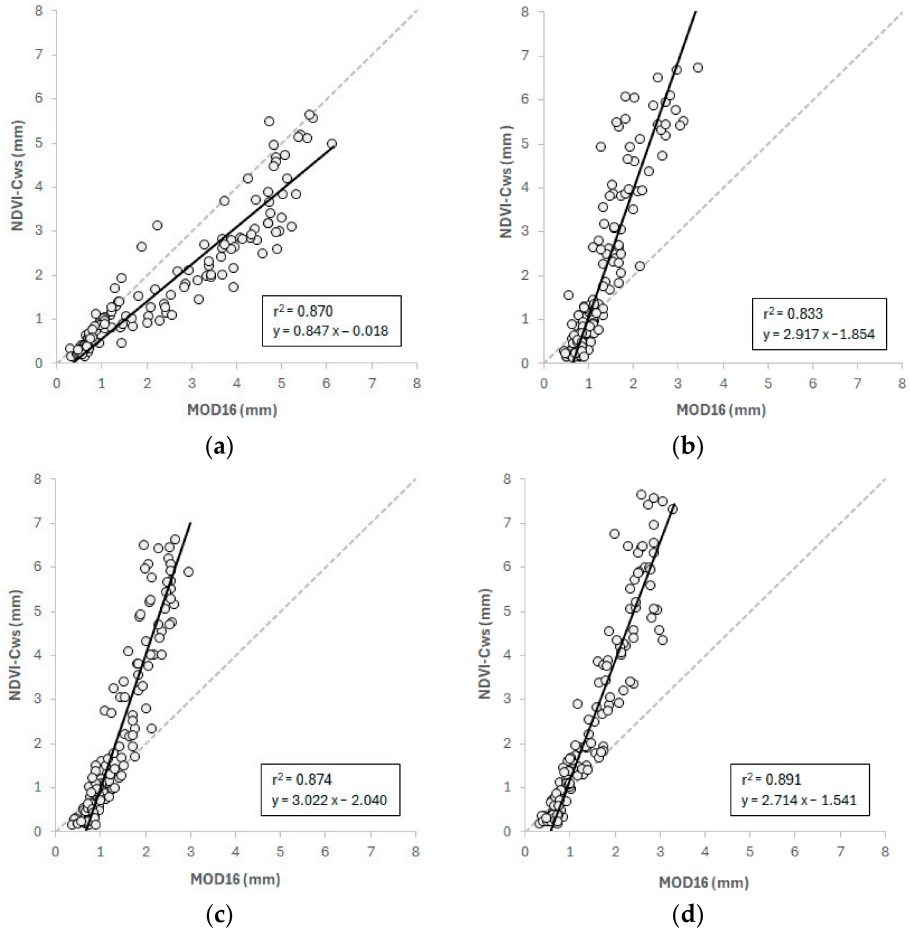


Figure 3. Scatter plots of the mean ETa values estimated over 8-day periods by MOD16 and NDVI-Cws for test site 1 ((**a**), forest), 3 ((**b**), grassland), 8 ((**c**), annual crop) and 9 ((**d**), annual crop mixed with perennial crop). The solid and dotted lines indicate the RMA regression and 1:1 fits, respectively. All correlations are statistically highly significant, $p < 0.01$.

Table 2. RMA regression statistics obtained in the dual intercomparison of the three ETa datasets for the six sites not considered in Figures 3 and 4. Table 2a refers to MOD16/NDVI-Cws while Table 2b refers to Sen-ET/NDVI-Cws. All correlations are statistically highly significant, $p < 0.01$.

(**a**)			
ID	**r^2**	**a**	**b**
2	0.909	1.650	−0.941
4	0.791	4.129	−2.710
5	0.819	3.467	−2.080
6	0.744	3.613	−2.275
7	0.818	3.916	−2.583
10	0.768	2.934	−1.870
(**b**)			
ID	**r^2**	**a**	**b**
2	0.828	0.956	−0.602
4	0.724	1.676	−1.685
5	0.777	1.651	−1.553
6	0.766	1.462	−1.266
7	0.725	1.700	−1.700
10	0.781	1.047	−0.651

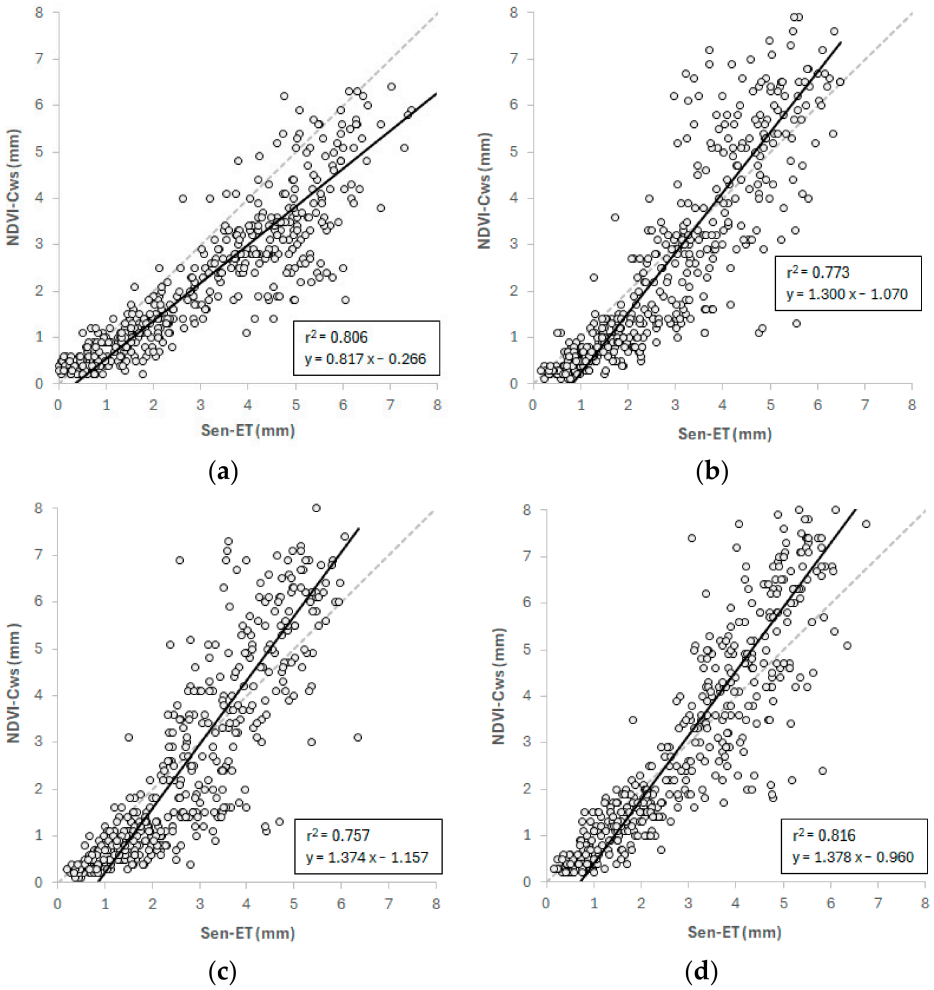


Figure 4. Scatter plots of the daily ETa values estimated by Sen-ET and NDVI-Cws for test site 1 ((**a**), forest), 3 ((**b**), grassland), 8 ((**c**), annual crop) and 9 ((**d**), annual crop mixed with perennial crop). The solid and dotted lines indicate the RMA regression and 1:1 fits, respectively. All correlations are statistically highly significant, $p < 0.01$.

4. Discussion

All remote sensing ETa estimation methods that have been proposed in recent decades present pros and cons attributable to both the algorithms and the drivers utilized. In view of an operational application of these methods, the main properties to consider in addition to the prediction accuracy are related to the spatial and temporal scales of observation and to the completeness of the obtained estimates.

Energy balance methods rely on a sound theoretical background but suffer from spatio-temporal resolution issues mainly caused by the characteristics of the input TIR imagery [42,43]. These issues have been partly overcome by the application of data fusion techniques which exploit the joint potential of TIR and shortwave satellite acquisitions [38]. A recent example of these methodologies is given by Sen-ET, which has been applied in the framework of the European Space Agency 4DMED-Hydrology project [30] following the approach proposed by Guzinski et al. [7].

Mixed remote sensing methods offer greater operational potential but have limited spatial and temporal resolutions and are relatively inefficient in specific environmental situations. This is the case for the classical MOD16 algorithm, which was developed over 25 years ago for global ET monitoring and shows variable performances in different climates and ecosystems [9]. Tang et al. [44], for example, found that this algorithm under-

estimates ETa in irrigated croplands, while Feng et al. [45] reported lower performances for semi-natural ecosystems in arid and semi-arid environments.

Conventional water balance methods are applicable in eco-climatic situations not affected by water scarcity but generally fail in properly accounting for the impact of WS [5]. The most recent versions of these methods, however, are capable of addressing this limitation by the proper elaboration of ancillary information. This is the case of the NDVI-Cws method, which has been successfully applied in Mediterranean regions covered by both semi-natural and agricultural vegetation [31].

The current investigation has performed an intercomparison of these three methods, each representative for the basic strategies mentioned above (energy balance, mixed, water balance). The analysis was conducted over a complex area of Northeast Italy partly covered by irrigated crops, with the aim of evaluating the consistency and differences among the datasets. The application of this strategy theoretically requires an assumption of statistical independence among the three estimated datasets [16], which can be currently considered reasonable. The three datasets, in fact, are obtained by algorithms that are based on different principles (i.e., Penman–Monteith for MOD16, energy balance for Sen-ET and water balance for NDVI-Cws) and are fed with different ancillary and remotely sensed drivers.

The results obtained by the experimental analyses are mostly in line with the aforementioned strengths and limitations of the main ETa estimation strategies as well as with the findings of previous assessments [9,38,46]. The analyses conducted over the ten selected test sites, in fact, indicate that the mean ETa estimates produced by MOD16 and NDVI-Cws are significantly different for all examined vegetation types and highly significantly different for non-forest sites. In the case of forests, the MOD16 algorithm yields ETa estimates which are partially and fully higher than those of NDVI-Cws and Sen-ET, respectively; the same estimates are much lower than those of the latter methods for all croplands and grasslands.

The Sen-ET and NDVI-Cws estimates are therefore the most similar in magnitude for all agricultural and mixed ecosystems (no statistically significant difference detected by Student's *t*-test). The marginally lower correlations found between Sen-ET and NDVI-Cws versus MOD16 and NDVI-Cws estimates can instead be attributed to the reduction in random variability caused in the latter case by the data aggregation over 8-day periods.

The RMA regression slopes found between Sen-ET and NDVI-Cws estimates, however, are higher than 1 for irrigated croplands, indicating that the temporal variances predicted by the former method are notably lower than those of the latter. Such finding can be likely attributed to the effects of the S-3 and S-2 data fusion, which induces a dampening of extreme LST and, consequently, ETa estimates [37].

This is expected to be particularly the case in spatially heterogeneous croplands, where adjacent irrigated and rainfed or bare fields can show very diversified LST values. Such an artefact is instead reduced in spatially homogeneous areas, where the mean plot size is comparable to the resolution of the LST imagery used.

These results indicate the higher similarity between the Sen-ET and NDVI-Cws estimates with respect to those of MOD16, which is noticeable considering the different nature of the former two algorithms. Sen-ET, in fact, is physically based and is therefore capable of predicting the actual energy and water fluxes of the observed land surface; this operation, however, depends on the availability of TIR datasets having appropriate spatio-temporal features, which is markedly improved by the applied data fusion technique [7,47]. The NDVI-Cws method instead utilizes a semi-empirical water balance approach that relies on the combination of ancillary data and NDVI imagery [14].

These characteristics allow the NDVI-Cws method to yield estimates which, being continuous and complete both in space and in time, are suitable for operational ETa monitoring at different time steps. An example map of ETa estimated over the study area

and an entire year (2021) is shown in Figure 5. Annual ETa ranges from about 200 mm in urban lands to 800–900 mm in irrigated croplands; forests show intermediate values.

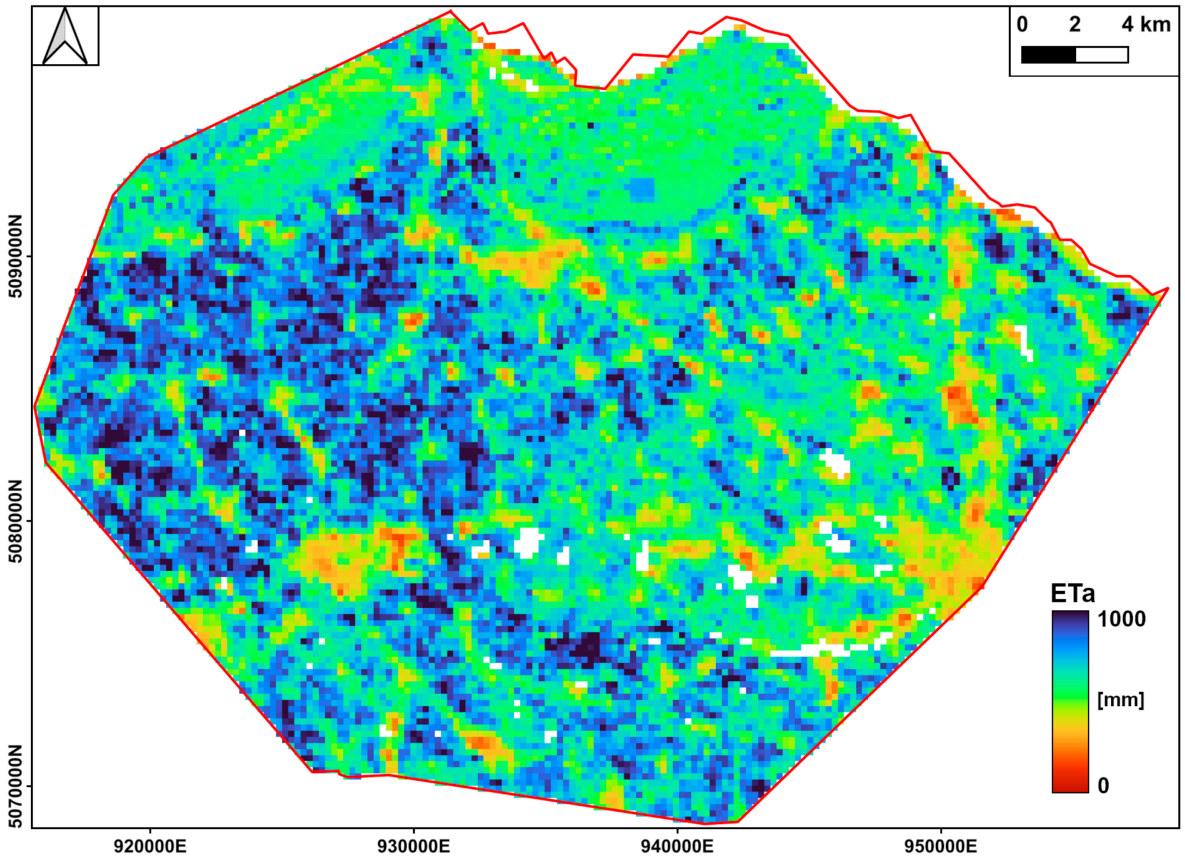


Figure 5. Example of the annual ETa map obtained applying the NDVI-Cws method for the last study year (2021) in the Venetian plain area; the masked-out pixels correspond to water bodies.

5. Conclusions

A comparative assessment of three remote sensing ETa estimation methods has been performed over a complex area in Northeast Italy covered by mixed forest and agricultural vegetation types. Specifically, the analysis has considered the MOD16 global evapotranspiration product, the Sen-ET energy balance algorithm and the NDVI-Cws water balance method.

The results obtained indicate that the ETa estimates produced by Sen-ET and NDVI-Cws are generally concordant, both in intensity and time evolution; this is less the case for the MOD16 estimates, which are much lower than the others in all croplands. These findings suggest that the first two algorithms may provide more reliable ETa estimates for the study area, where irrigated crops are prevalent. The NDVI-Cws method, however, is the only one that can produce complete and continuous daily ETa estimates (and therefore water needed for irrigation) at a spatial resolution which is mainly dependent on the NDVI imagery used. The outputs of this method could also be fused and/or integrated with those of other algorithms, following the strategy proposed by Melton et al. [48] to improve ETa prediction confidence. In particular, the combination of NDVI-Cws and Sen-ET outputs could be seen as a suitable means to overcome most of the theoretical and practical issues of the two methods.

Author Contributions: Conceptualization, F.M. and C.M.; methodology, F.M. and C.M.; software, L.F. and P.B.; validation, M.C. (Marta Chiesi), C.M. and L.F.; formal analysis, J.D. and S.V.; inves-

tigation, M.C. (Marta Chiesi) and M.P.; data curation, S.O., M.C. (Mariapina Castelli) and B.G.; writing—original draft preparation, F.M.; writing—review and editing, C.M., M.C. (Matteo Camporese), M.C. (Marta Chiesi) and L.F.; visualization, M.P.; supervision, F.M. All authors have read and agreed to the published version of the manuscript.

Funding: This research received no external funding.

Data Availability Statement: Data will be available on request to the corresponding author.

Acknowledgments: The Sen-ET product was generated within the framework of the 4DMED-Hydrology project. This work was supported by the AQUIGROW project (www.aquigrow.it; accessed on 25 May 2026), funded under the Water4All Partnership (co-funded by the European Union) through the Joint Transnational Call 2022, with funding provided by MUR (Italy), ANR (France), MoE (Israel), NCBR (Poland), and DSTI (South Africa). The authors wish to thank the three anonymous *Hydrology* reviewers for their insightful comments on the first draft of the manuscript.

Conflicts of Interest: The authors declare no conflicts of interest.

Abbreviations

The following abbreviations related to the Sen-ET algorithm are used in this manuscript:

ET	Evapotranspiration (mm d^{-1})
LE	Latent heat flux (W m^{-2})
LEc	Canopy latent heat flux (W m^{-2})
LEs	Soil latent heat flux (W m^{-2})
LE_{daily}	Daily latent heat flux extrapolated to 24 h (W m^{-2})
H	Sensible heat flux (W m^{-2})
Hs	Soil sensible heat flux (W m^{-2})
G	Soil heat flux (W m^{-2})
Rn	Net radiation (W m^{-2})
Rnc	Canopy net radiation (W m^{-2})
Rns	Soil net radiation (W m^{-2})
LST	Land surface temperature (K)
LST_C	Canopy temperature (K)
LST_S	Soil temperature (K)
f_C	Fractional vegetation cover (–)
f_G	Fraction of green vegetation (–)
LAI	Leaf area index (m^2 m^{-2})
VZA	Satellite view zenith angle (°)
R_a	Aerodynamic resistance to heat transfer (s m^{-1})
R_x	Canopy boundary layer resistance (s m^{-1})
R_s	Soil surface resistance (s m^{-1})
α_{PT}	Priestley–Taylor coefficient (default = 1.26) (–)
Δ	Slope of the saturation vapour pressure curve (kPa K^{-1})
Γ	Psychrometric constant (kPa K^{-1})
ε_C	Canopy emissivity (–)
ε_S	Soil emissivity (–)

Appendix A

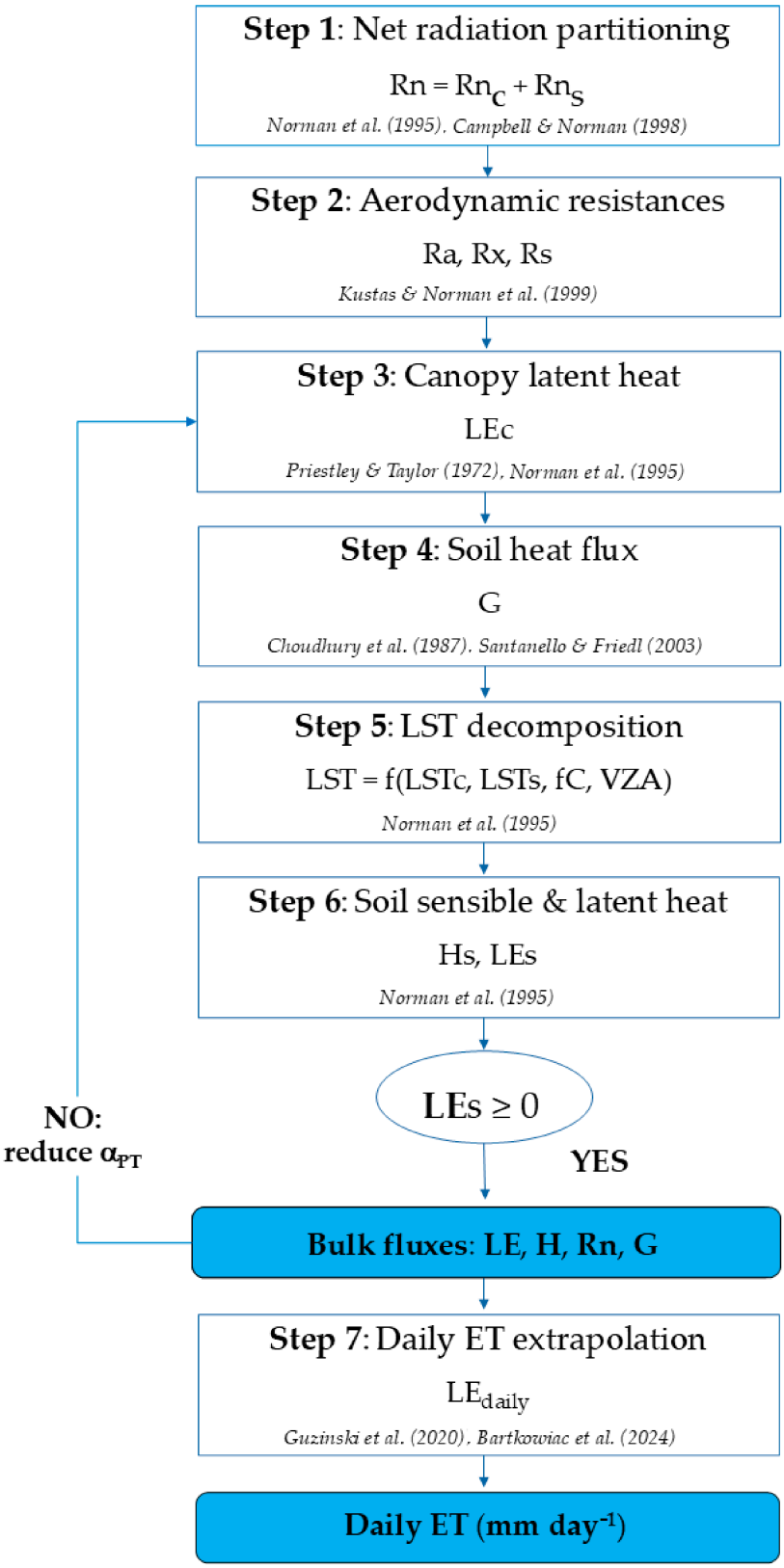


Figure A1. Scheme of Sen-ET functioning (see Section 2.3.2). Norman et al. (1995) [26]; Campbell and Norman (1998) [49]; Kusta and Norman (1999) [27]; Priestley and Taylor (1972) [28]; Choudhuri et al. (1987) [50]; Santarello and Friedel (2003) [51]; Guzinski et al. (2020) [7]; Bartkowiak et. (2024) [30].

References

1. Allen, R.G.; Pereira, L.S.; Raes, D.; Smith, M. *Crop Evapotranspiration—Guidelines for Computing Crop Water Requirements*; FAO Irrigation and drainage paper 56; FAO—Food and Agriculture Organization of the United Nations: Rome, Italy, 1998; p. 300. Available online: http://www.fao.org/docrep/x0490e/x0490e00.htm (accessed on 25 April 2026).
2. Allen, R.; Irmak, A.; Trezza, R.; Hendrickx, J.M.H.; Bastiaanssen, W.G.M.; Kjaersgaard, J. Satellite-based ET estimation in agriculture using SEBAL and METRIC. *Hydrol. Process.* **2011**, *25*, 4011–4027. [CrossRef]
3. Senay, G.B.; Bohms, S.; Verdin, J.P. Remote sensing of evapotranspiration for operational drought monitoring using principles of water and energy balance. In *Remote Sensing of Drought: Innovative Monitoring Approaches*; Wardlow, B.D., Anderson, M.C., Verdin, J.P., Eds.; Taylor & Francis Group: Boca Raton, FL, USA, 2012; pp. 123–144. [CrossRef]
4. Cammalleri, C.; Anderson, M.C.; Ciraolo, G.; D'Urso, G.; Kustas, W.P.; La Loggia, G.; Minacapilli, M. Applications of a remote sensing-based two-source energy balance algorithm for mapping surface fluxes without in situ air temperature observations. *Remote Sens. Environ.* **2012**, *124*, 502–515. [CrossRef]
5. Glenn, E.P.; Nagler, P.L.; Huete, A.R. Vegetation index methods for estimating evapotranspiration by remote sensing. *Surv. Geophys.* **2010**, *31*, 531–555. [CrossRef]
6. Volk, J.M.; Huntington, J.L.; Melton, F.S.; Allen, R.; Anderson, M.; Fisher, J.B.; Kilic, A.; Ruhoff, A.; Senay, G.B.; Minor, B.; et al. Assessing the accuracy of OpenET satellite-based evapotranspiration data to support water resource and land management applications. *Nat. Water* **2024**, *2*, 193–205. [CrossRef]
7. Guzinski, R.; Nieto, H.; Sandhold, I.; Karamitilios, G. Modelling high-resolution actual evapotranspiration through Sentinel-2 and Sentinel-3 data fusion. *Remote Sens.* **2020**, *12*, 1433. [CrossRef]
8. Mu, Q.; Zhao, M.; Running, S.W. Improvements to a MODIS global terrestrial evapotranspiration algorithm. *Remote Sens. Environ.* **2011**, *115*, 1781–1800. [CrossRef]
9. Hu, G.; Jia, L.; Menenti, M. Comparison of MOD16 and LSA-SAF MSG evapotranspiration products over Europe for 2011. *Remote Sens. Environ.* **2015**, *156*, 510–526. [CrossRef]
10. Senay, G.B. Modeling Landscape Evapotranspiration by Integrating Land Surface Phenology and a Water Balance Algorithm. *Algorithms* **2008**, *1*, 52–68. [CrossRef]
11. Rocha, J.; Perdigao, A.; Melo, R.; Henriques, C. Remote sensing based crop coefficients for water management in agriculture. In *Sustainable Development—Authoritative and Leading Edge Content for Environmental Management*; Curkovic, S., Ed.; IntechOpen: London, UK, 2012. [CrossRef]
12. Maselli, F.; Papale, D.; Puletti, N.; Chirici, G.; Corona, P. Combining remote sensing and ancillary data to monitor the gross productivity of water-limited forest ecosystems. *Remote Sens. Environ.* **2009**, *113*, 657–667. [CrossRef]
13. Senay, G.B.; Kagone, S.; Parrish, G.E.L.; Khand, K.; Boiko, O.; Velpuri, N.M. Improvements and evaluation of the agro-hydrologic VegET model for large-area water budget analysis and drought monitoring. *Hydrology* **2023**, *10*, 168. [CrossRef]
14. Maselli, F.; Papale, D.; Chiesi, M.; Matteucci, G.; Angeli, L.; Raschi, A.; Seufert, G. Operational monitoring of daily evapotranspiration by the combination of MODIS NDVI and ground meteorological data: Application and validation in Central Italy. *Remote Sens. Environ.* **2014**, *152*, 279–290. [CrossRef]
15. Baldocchi, D. Measuring fluxes of trace gases and energy between ecosystems and the atmosphere—The state and future of the eddy covariance method. *Glob. Change Biol.* **2014**, *20*, 3600–3609. [CrossRef]
16. Stoffelen, A. Toward the true near-surface wind speed: Error modeling and calibration using triple collocation. *J. Geophys. Res. Ocean.* **1998**, *103*, 7755–7766. [CrossRef]
17. Gatto, B.; Furlanetto, D.; Camporese, M.; Trentin, T.; Salandin, P. Quantifying groundwater recharge in the Venetian high plain between the Brenta and Piave Rivers through integrated surface–subsurface hydrological modeling. *J. Hydrol. Reg. Stud.* **2023**, *50*, 101550. [CrossRef]
18. Copernicus Sentinel-3 SLSTR Land User Handbook. European Space Agency (ESA). Available online: https://sentinels.copernicus.eu/documents/247904/4598082/Sentinel-3-SLSTR-Land-Handbook.pdf (accessed on 18 March 2026).
19. Hersbach, H.; Bell, B.; Berrisford, P.; Hirahara, S.; Horányi, A.; Muñoz-Sabater, J.; Nicolas, J.; Peubey, C.; Radu, R.; Schepers, D.; et al. The ERA5 global reanalysis. *Q. J. R. Meteorol. Soc.* **2020**, *146*, 1999–2049. [CrossRef]
20. NASA JPL. NASA Shuttle Radar Topography Mission Global 1 Arc Second V003, NASA Land Processes DAAC. 2013. Available online: https://www.earthdata.nasa.gov/data/catalog/lpcloud-srtmgl1-003 (accessed on 25 April 2026).
21. Reinhart, V.; Fonte, C.C.; Hoffmann, P.; Bechtel, B.; Rechid, D.; Böhner, J. Comparison of ESA climate change initiative land cover to CORINE land cover over Eastern Europe and the Baltic States from a regional climate modeling perspective. *Int. J. Appl. Earth Obs. Geoinf.* **2021**, *94*, 102221. [CrossRef]
22. World Meteorological Organization (WMO). *Guide to Instruments and Methods of Observation*; WMO-No. 8; WMO: Geneva, Switzerland, 2024; Volume I.
23. Fibbi, L.; Maselli, F.; Pieri, M. Improved estimation of global solar radiation over rugged terrains by the disaggregation of Satellite Applications Facility on Land Surface Analysis data (LSA SAF). *Meteorol. Appl.* **2020**, *27*, e1940. [CrossRef]

24. Running, S.W.; Mu, Q.; Zhao, M.; Moreno, A. *User's Guide MODIS Global Terrestrial Evapotranspiration (ET) Product (MOD16A2/A3 and Year-End Gap-Filled MOD16A2GF/A3GF) NASA Earth Observing System MODIS Land Algorithm (for Collection 6.1)*; MODIS Land Algorithm Team: Washington, DC, USA, 2021. Available online: https://modis-land.gsfc.nasa.gov/pdf/MOD16C61UsersGuideV10Feb2021.pdf (accessed on 25 April 2026).
25. He, M.; Kimball, J.S.; Yi, Y.; Running, S.W.; Guan, K.; Moreno, A.; Wu, X.; Maneta, M. Satellite data-driven modeling of field scale evapotranspiration in croplands using the MOD16 algorithm framework. *Remote Sens. Environ.* **2019**, *230*, 111201. [CrossRef]
26. Norman, J.M.; Kustas, W.P.; Humes, K.S. Source approach for estimating soil and vegetation energy fluxes in observations of directional radiometric surface temperature. *Agric. For. Meteorol.* **1995**, *77*, 263–293. [CrossRef]
27. Kustas, W.P.; Norman, J.M. Evaluation of soil and vegetation heat flux predictions using a simple two-source model with radiometric temperatures for partial canopy cover. *Agric. For. Meteorol.* **1999**, *94*, 13–29. [CrossRef]
28. Priestley, C.H.B.; Taylor, R.J. On the assessment of surface heat flux and evaporation using large-scale parameters. *Mon. Weather Rev.* **1972**, *100*, 81–92. [CrossRef]
29. Chintala, S.; Harmya, T.S.; Kambhammettu, B.V.N.P.; Moharana, S.; Duvvuri, S. Modelling high-resolution Evapotranspiration in fragmented croplands from the constellation of Sentinels. *Remote Sens. Appl. Soc. Environ.* **2022**, *26*, 100704. [CrossRef]
30. Bartkowiak, P.; Ventura, B.; Jacob, A.; Castelli, M. A Copernicus-based evapotranspiration dataset at 100 m spatial resolution over four Mediterranean basins. *Earth Syst. Sci. Data* **2024**, *16*, 4709–4734. [CrossRef]
31. Maselli, F.; Battista, P.; Chiesi, M.; Rapi, B.; Angeli, L.; Fibbi, L.; Magno, R.; Gozzini, B. Use of Sentinel-2 MSI data to monitor crop irrigation in Mediterranean areas. *Int. J. Appl. Earth Obs. Geoinf.* **2020**, *93*, 102216. [CrossRef]
32. Jensen, M.E.; Haise, H.R. Estimating evapotranspiration from solar radiation. *J. Irrig. Drain. Div.* **1963**, *89*, 15–41. [CrossRef]
33. Gutman, G.; Ignatov, A. The derivation of the green vegetation fraction from NOAA/AVHRR data for use in numerical weather prediction models. *Int. J. Remote Sens.* **1998**, *19*, 1533–1543. [CrossRef]
34. Weiss, M.; Baret, F. S2ToolBox Level 2 products: LAI, FAPAR, FCOVER. In *Sentinel2 ToolBox Level2 Products*; ESA: Paris, France, 2016. Available online: https://step.esa.int/docs/extra/ATBD_S2ToolBox_L2B_V1.1.pdf (accessed on 25 April 2026).
35. Guzinski, R.; Nieto, H.; Sanchez, J.M.; Lopez-Urrea, R.; Boujnah, D.M.; Boulet, G. Utility of Copernicus-based inputs for actual evapotranspiration modeling in support of sustainable water use in agriculture. *IEEE J. Sel. Top. Appl. Earth Obs. Remote Sens.* **2021**, *14*, 11466–11484. [CrossRef]
36. Gao, F.; Kustas, W.P.; Anderson, M.C. A data mining approach for sharpening thermal satellite imagery over land. *Remote Sens.* **2012**, *4*, 3287–3319. [CrossRef]
37. Guzinski, R.; Nieto, H.; Sánchez, R.R.; Sánchez, J.M.; Jomaa, I.; Zitouna-Chebbi, R.; Roupsard, O.; López-Urrea, R. Improving field-scale crop actual evapotranspiration monitoring with Sentinel-3, Sentinel-2, and Landsat data fusion. *Int. J. Appl. Earth Obs. Geoinf.* **2023**, *125*, 103587. [CrossRef]
38. Guzinski, R.; Nieto, H. Evaluating the feasibility of using Sentinel-2 and Sentinel-3 satellites for high-resolution evapotranspiration estimations. *Remote Sens. Environ.* **2019**, *221*, 157–172. [CrossRef]
39. Massari, C.; Tarpanelli, A.; Aires, F.; Alfieri, L.; Avanzi, F.; Barbetta, S.; Bechtold, M.; Brocca, L.; Camici, S.; Castelli, M.; et al. 4DMED-Hydrology: Capitalizing high resolution Earth Observation data for a consistent reconstruction of the Mediterranean terrestrial water cycle [Poster Presentation]. In Proceedings of the ESA Living Planet Symposium 2022, Bonn, Germany, 23–27 May 2022.
40. Chiesi, M.; Angeli, L.; Battista, P.; Fibbi, L.; Rapi, B.; Gozzini, B.; Maselli, F. Monitoring and analysis of crop irrigation dynamics in Central Italy through the use of MODIS NDVI data. *Eur. J. Remote Sens.* **2022**, *55*, 23–36. [CrossRef]
41. Harper, W.V. Reduced major axis regression. In *Wiley StatsRef: Statistics Reference Online*; Balakrishnan, N., Colton, T., Everitt, B., Piegorsch, W., Ruggeri, F., Teugels, J.L., Eds.; Wiley Online Library: Hoboken, NJ, USA, 2016. [CrossRef]
42. Zhang, K.; Kimball, J.S.; Running, S.W. A review of remote sensing based actual evapotranspiration estimation. *WIREs Water* **2016**, *3*, 834–853. [CrossRef]
43. Delogu, E.; Olioso, A.; Alliès, A.; Demarty, J.; Boulet, G. Evaluation of multiple Methods for the production of continuous evapotranspiration estimates from TIR remote sensing. *Remote Sens.* **2021**, *13*, 1086. [CrossRef]
44. Tang, R.L.; Shao, K.; Li, Z.L.; Wu, H.; Tang, B.H.; Zhou, G.Q.; Zhang, L. Multiscale validation of the 8-day MOD16 evapotranspiration product using flux data collected in China. *IEEE J. Sel. Top. Appl. Earth Obs. Remote Sens.* **2015**, *8*, 1478–1486. [CrossRef]
45. Feng, F.; Chen, J.Q.; Li, X.L.; Yao, Y.J.; Liang, S.L.; Liu, M.; Zhang, N.N.; Guo, Y.; Yu, J.; Sun, M.M. Validity of five satellite-based latent heat flux algorithms for semi-arid ecosystems. *Remote Sens.* **2015**, *7*, 16733–16755. [CrossRef]
46. Fibbi, L.; Chiesi, M.; Pieri, M.; Bartolini, G.; Grifoni, D.; Gozzini, B.; Maselli, F. Assessment of three remote sensing methods for estimating actual evapotranspiration in a Mediterranean region. *Int. J. Appl. Earth Obs. Geoinf.* **2026**, *146*, 105003. [CrossRef]
47. Garcia-Santos, V.; Sánchez, J.M.; Cuxart, J. Evapotranspiration acquired with remote sensing thermal-based algorithms: A state-of-the-art review. *Remote Sens.* **2022**, *14*, 3440. [CrossRef]

48. Melton, F.S.; Huntington, J.; Grimm, R.; Herring, J.; Hall, M.; Rollison, D.; Erickson, T.; Allen, R.; Anderson, M.; Fisher, J.B.; et al. OpenET: Filling a critical data gap in water management for the Western United States. *J. Am. Water Resour. Assoc.* **2022**, *58*, 971–994. [CrossRef]
49. Campbell, G.S.; Norman, J.M. Radiation fluxes in natural environments. In *An Introduction to Environmental Biophysics*; Springer: New York, NY, USA, 1998; pp. 167–184. [CrossRef]
50. Choudhury, B.J.; Idso, S.B.; Reginato, R.J. Analysis of an empirical model for soil heat flux under a growing wheat crop for estimating evaporation by an infrared-temperature based energy balance equation. *Agric. For. Meteorol.* **1987**, *39*, 283–297. [CrossRef]
51. Santanello, J.A.; Friedl, M.A. Diurnal covariation in soil heat flux and net radiation. *J. Appl. Meteorol.* **2003**, *42*, 851–862. [CrossRef]

Disclaimer/Publisher's Note: The statements, opinions and data contained in all publications are solely those of the individual author(s) and contributor(s) and not of MDPI and/or the editor(s). MDPI and/or the editor(s) disclaim responsibility for any injury to people or property resulting from any ideas, methods, instructions or products referred to in the content.